Progress In Electromagnetics Research, PIER 58, 115–133, 2006

RADIATION PATTERN OF APERTURE COUPLED PROLATE HEMISPHEROIDAL DIELECTRIC RESONATOR ANTENNA

Y. Song and A. R. Sebak

Department of Electrical and Computer Engineering
Concordia University
Montreal, Quebec, H3G 1M8, Canada

Abstract—An analytical solution for the radiation by a prolate hemispheroidal dielectric resonator antenna (DRA) over an infinite ground plane excited by a rectangular slot is presented. The dyadic Green's functions pertaining to a magnetic-current source are used in a form convenient for numerical computations. The dyadic Green's functions are then employed to formulate the electromagnetic fields radiated by the DRA. The electromagnetic far field is expressed analytically in a compact form. The far field patterns for different design parameters are computed and plotted.

1. INTRODUCTION

Since the early experimental study of dielectric resonator antenna (DRA) by Long, McAllister and others [1–3], the dielectric resonator antennas have been studied extensively. It has been shown that DRAs can be used as effective radiators at microwave frequencies where ohmic losses become a serious problem for conventional metallic antennas. DRAs offer a number of advantages such as small size, lightweight, low cost, ease of excitation, and ease of integration with active circuitry. Furthermore, they offer wider bandwidth than the microstrip patch antennas commonly used at the same frequency range [4].

Various shapes of the DRA have been investigated in the past two decades such as hemispherical DRAs [5–9], cylindrical DRAs [10–14], rectangular DRAs [2, 15, 16] and triangular DRAs [17, 18]. One of the most useful DRAs is the hemispherical DRA. Compared with hemispherical DRAs, hemispheroidal DRAs are potentially attractive. They add one more design parameter in terms of different semi-axes dimensions and may lead to a simple feeding mechanism for

generating circularly polarized waves. Another parameter that may lead to a better performance is the diversity of mode excitation than hemispherical DRAs. Canonical structures, including spheroidal geometries, require no magnetic wall assumption in the problem formulation and hence an accurate solution can be obtained. The analysis of the radiation characteristics of hemispheroidal DRA is very complicated. The difficulty is mainly due to two aspects. One is the very complicated calculation of the spheroidal angular and radial functions. The other is the lack of orthogonality of spheroidal vector wave functions. This is part of the reason that there have been fewer reports about the applications of spheroidal wave functions in computational electromagnetic than those related to other canonical geometries.

In this paper, we present an analytical solution for the radiation by a prolate hemispheroidal DRA over an infinite ground plane using a dyadic Green's function technique. The aperture-coupled prolate hemispheroidal DRA excited at the fundamental broadside TE_{111} mode is shown in Fig. 1. In Section 2, the dyadic Green's functions pertaining to a magnetic-current source located in a dielectric prolate spheroid is briefly presented. The modal series is represented as a sum of unbounded and scattering solutions. Both solutions are expressed in terms of proper vector spheroidal wave functions with unknown scattering expansion coefficients. The unbounded solution alone represents the source radiating in the unbounded dielectric medium, while the scattering solution accounts for the presence of the dielectric discontinuity. The unknown scattering coefficients of the dyadic Green's functions are obtained by enforcing the boundary conditions. The scattering coefficients of each of the scattering dyadic Green's functions are coupled with one another. The coupled system of linear equations satisfied by these coefficients is obtained. The unknown scattering coefficients are expressed in terms of integrals of the current source on the slot. In this paper the slot current distribution is assumed and approximated by a dominant TE_{111} mode. The formulation of electromagnetic far fields are expressed in terms of dyadic Green's functions and simplified using the asymptotic form of the spheroidal radial function. A compact form of the electric far field is obtained. In Section 3, the antenna radiation patterns are computed numerically for different design parameters. The accuracy of the solution is checked by comparing with Ansoft HFSS [19] simulation results and published data for the special case of a hemispherical DRA [9] when the axial ratio b/a of the hemispheroid approaches one. In Section 4, conclusions are summarized.

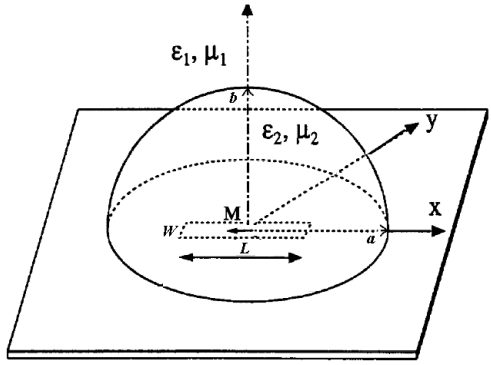

Figure 1. Configuration of the hemispheroidal DRA excited by a slot.

2. FORMULATION

The geometry of the hemi-spheroidal DRA is shown in Fig. 1, where a and b are the semi-minor and major axes. The slot length is L and its narrow width is W. The dyadic Green's function technique is usually adopted to analyze the electromagnetic radiation from an arbitrary current distribution located in a layered homogeneous medium, For the spheroidal geometry, the representation of dyadic Green's function (DGF) in the spheroidal coordinate system is most convenient. When the source current distribution is known, the electromagnetic fields can be integrated directly from DGF, which plays an important role as the response function of multi-layered dielectric media. If the source is an unknown current distribution, the method of moments can be employed. In this case, the DGF is considered as a kernel of the integral; and the unknown coefficients of the basis functions can be obtained by enforcing the boundary conditions.

In this work, the dyadic Green's functions pertaining to a slot source inside a dielectric prolate hemi-spheroid, as shown in Fig. 1, is used. The ground plane in Fig. 1 is assumed infinite. The half space is divided by the interface of $\xi = \xi_0$ into region 1 and region 2. Region 1 is characterized by permittivity ε_1 and permeability μ_1, and region 2 is characterized by permittivity ε_2 and permeability μ_2. Image theory permits the removal of the ground plane by placing a virtual image source on the other side of the ground plane. The equivalent problem of Fig. 1 is obtained by applying the image theory, and is shown in Fig. 2. The dyadic Green's functions $\overline{\boldsymbol{G}}_{\substack{e \\ m^2}}(\boldsymbol{r}, \boldsymbol{r}')$ pertaining to a magnetic-current source are called the electric and magnetic dyadic Green's function of the second kind according to Tai [20]. The EM

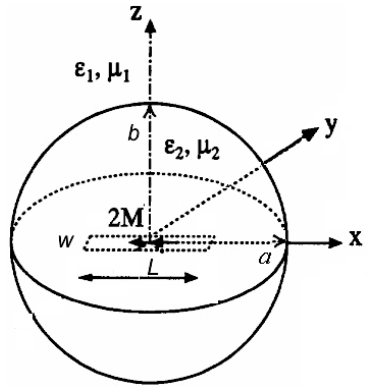

Figure 2. Equivalent problems for the hemispheroidal DRA in Fig. 1, excited by a slot.

fields inside and outside the spheroid can be expressed in terms of the spheroidal dyadic Green's functions and an arbitrary current source distribution.

Using the principle of scattering superposition [21], the dyadic Green's functions can be considered as the sum of the unbounded dyadic Green's function and scattering dyadic Green's functions. The unbounded solution represents the source radiating in the unbounded dielectric medium, while the scattering solution accounts for the presence of the dielectric discontinuity. The unbounded dyadic Green's functions under prolate spheroidal coordinates are formulated in terms of prolate spheroidal vector wave functions $\boldsymbol{M}^{a(i)}_{\substack{e\\o}mn}$ and $\boldsymbol{N}^{a(i)}_{\substack{e\\o}mn}$ ($a = x, y, z$; and $i = 1, 2, 3$). The scattering dyadic Green's functions are formulated using the method originally developed by Tai [20] and later by Li *et al.*, [20]. Scattering coefficients of each of the scattering dyadic Green's functions are coupled with one another. The coupled system of linear equations satisfied by these coefficients is constructed under the requirements of the boundary conditions, and can be solved numerically.

2.1. General Formula

The EM radiation fields $\boldsymbol{E}_f$ and $\boldsymbol{H}_f$ in region f ($f = 1, 2$), due to magnetic current source $\boldsymbol{M}_s$ located in region 2 are expressed by

$$\nabla \times \nabla \times \boldsymbol{E}_f - k_f^2 \boldsymbol{E}_f = (-\nabla \times \boldsymbol{M}_s)\delta_{f2} \quad (1)$$

$$\nabla \times \nabla \times \boldsymbol{H}_f - k_f^2 \boldsymbol{H}_f = (i\omega\varepsilon_f \boldsymbol{M}_s)\delta_{f2} \quad (2)$$

where δ_{f2} is the Kronecker delta ($\delta_{f2} = 1$ for $f = 2$ and 0 for $f = 1$); $k_f = \omega\sqrt{\mu_f \varepsilon_f}$ is the propagation constant in region f. The time dependent factor $e^{-i\omega t}$ is assumed throughout this paper.

The EM field excited by a magnetic current source $\boldsymbol{M}_s$ in region 2 can be expressed in term of dyadic Green's functions as

$$\boldsymbol{E}_f(\boldsymbol{r}) = -\iiint_v \overline{\boldsymbol{G}}_{m2}^{(f)}(\boldsymbol{r}, \boldsymbol{r}') \cdot \boldsymbol{M}_s(\boldsymbol{r}')dv' \tag{3}$$

$$\boldsymbol{H}_f(\boldsymbol{r}) = i\omega\varepsilon_f \iiint_v \overline{\boldsymbol{G}}_{e2}^{(f)}(\boldsymbol{r}, \boldsymbol{r}') \cdot \boldsymbol{M}_s(\boldsymbol{r}')dv' \tag{4}$$

where denotes the coordinates (ξ, ν, ϕ) at the field point; $\boldsymbol{r}'$ denotes the coordinates (ξ, ν, ϕ) of the magnetic current source $\boldsymbol{M}_s$; v denotes the volume occupied by the source in region 2; $\overline{\boldsymbol{G}}_{m2}^{(f)}(\boldsymbol{r}, \boldsymbol{r}')$ denotes the magnetic dyadic Green's function of the second kind; $\overline{\boldsymbol{G}}_{e2}^{(f)}(\boldsymbol{r}, \boldsymbol{r}')$ denotes the electric dyadic Green's function of the second kind. The superscript (f) denotes the dyadic Green's function in region 1 or region 2.

The electric and magnetic Dyadic Green's functions of the second kind $\overline{\boldsymbol{G}}_{m2}^{(f)}(\boldsymbol{r}, \boldsymbol{r}')$ and $\overline{\boldsymbol{G}}_{e2}^{(f)}(\boldsymbol{r}, \boldsymbol{r}')$ are related as

$$\nabla \times \overline{\boldsymbol{G}}_{e2}^{(f)}(\boldsymbol{r}, \boldsymbol{r}') = \overline{\boldsymbol{G}}_{m2}^{(f)}(\boldsymbol{r}, \boldsymbol{r}') \tag{5}$$

$$\nabla \times \overline{\boldsymbol{G}}_{m2}^{(f)}(\boldsymbol{r}, \boldsymbol{r}') = k_f^2 \overline{\boldsymbol{G}}_{e2}^{(f)}(\boldsymbol{r}, \boldsymbol{r}') + \overline{\boldsymbol{I}}\delta(\boldsymbol{r}, \boldsymbol{r}') \tag{6}$$

where $\overline{\boldsymbol{I}}$ is the unit dyad and $\delta(\boldsymbol{r}, \boldsymbol{r}')$ is the three-dimensional Dirac delta function.

Since the electric dyadic Green's functions $\overline{\boldsymbol{G}}_{e2}^{(f)}(\boldsymbol{r}, \boldsymbol{r}')$ can be obtained simply from the magnetic dyadic Green's functions $\overline{\boldsymbol{G}}_{m2}^{(f)}(\boldsymbol{r}, \boldsymbol{r}')$ using equation (5) or (6), we need only to solve the magnetic dyadic Green's functions $\overline{\boldsymbol{G}}_{m2}^{(f)}(\boldsymbol{r}, \boldsymbol{r}')$. The magnetic dyadic Green's function of the second kind $\overline{\boldsymbol{G}}_{m2}^{(f)}(\boldsymbol{r}, \boldsymbol{r}')$ satisfies the following boundary conditions at the spheroid interface ($\xi = \xi_0$):

$$\hat{\xi} \times \overline{\boldsymbol{G}}_{m2}^{(1)} = \hat{\xi} \times \overline{\boldsymbol{G}}_{m2}^{(2)} \tag{7}$$

$$\frac{1}{\varepsilon_1}\hat{\xi} \times \nabla \times \overline{\boldsymbol{G}}_{m2}^{(1)} = \frac{1}{\varepsilon_2}\hat{\xi} \times \nabla \times \overline{\boldsymbol{G}}_{m2}^{(2)}. \tag{8}$$

At the spheroid interface ($\xi = \xi_0$), the tangential components of both electric and magnetic fields are continuous. The boundary

conditions can be expressed as

$$\hat{\xi} \times \boldsymbol{E}_1 = \hat{\xi} \times \boldsymbol{E}_2 \tag{9}$$

$$\frac{1}{\mu_1}\hat{\xi} \times \nabla \times \boldsymbol{E}_1 = \frac{1}{\mu_2}\hat{\xi} \times \nabla \times \boldsymbol{E}_2. \tag{10}$$

Substituting equations (3) into equations (9) and (10), the result is

$$\hat{\xi} \times \iiint_v \overline{\boldsymbol{G}}^{(1)}_{m2}(\boldsymbol{r}, \boldsymbol{r}') \bullet \boldsymbol{M}_s(\boldsymbol{r}')dv' = \hat{\xi} \times \iiint_v \overline{\boldsymbol{G}}^{(2)}_{m2}(\boldsymbol{r}, \boldsymbol{r}') \bullet \boldsymbol{M}_s(\boldsymbol{r}')dv' \tag{11}$$

$$\frac{1}{\mu_1}\hat{\xi} \times \nabla \times \iiint_v \overline{\boldsymbol{G}}^{(1)}_{m2}(\boldsymbol{r}, \boldsymbol{r}') \bullet \boldsymbol{M}_s(\boldsymbol{r}')dv' = \frac{1}{\mu_2}\hat{\xi} \times \nabla \times \iiint_v \overline{\boldsymbol{G}}^{(2)}_{m2}(\boldsymbol{r}, \boldsymbol{r}') \bullet \boldsymbol{M}_s(\boldsymbol{r}')dv'. \tag{12}$$

Using the principle of scattering superposition, the dyadic Green's function can be considered as the sum of the unbounded Green's dyadic and the scattering dyadic Green's functions to be determined. The dyadic Green's functions are therefore given by

$$\overline{\boldsymbol{G}}^{(1)}_{m2}(\boldsymbol{r}, \boldsymbol{r}') = \overline{\boldsymbol{G}}^{(2)}_{ms}(\boldsymbol{r}, \boldsymbol{r}') \tag{13}$$

$$\overline{\boldsymbol{G}}^{(2)}_{m2}(\boldsymbol{r}, \boldsymbol{r}') = \overline{\boldsymbol{G}}_{m0}(\boldsymbol{r}, \boldsymbol{r}') + \overline{\boldsymbol{G}}^{(2)}_{ms}(\boldsymbol{r}, \boldsymbol{r}') \tag{14}$$

where the scattering dyadic Green's function $\overline{\boldsymbol{G}}^{(f)}_{ms}(\boldsymbol{r}, \boldsymbol{r}')$ represents the scattered-wave portion of the field due to the discontinuity of the boundary while the unbounded dyadic Green's function, $\overline{\boldsymbol{G}}_{m0}(\boldsymbol{r}, \boldsymbol{r}')$, represents the contribution of the direct waves from radiating sources in an unbounded medium. The subscript (s) denotes the scattering dyadic Green's functions. Detailed expressions for the above types of dyadic Green's functions are given in [21, 22]. The dyadic Green's functions are then used to determine the unknown scattering coefficients of the dyadic Green's functions as shown in the next section.

2.2. Calculation of the Scattering Coefficients

In equations (13) and (14), the dyadic Green's functions in terms of appropriate prolate spheroidal vector wave functions using the principle of scattering superposition are formulated. Because of the lack of general orthogonality of the spheroidal vector wave functions, the dyadic Green's functions are expressed in a different way, where

the coordinate unit vectors also combined in the construction of the solution. The unknown scattering coefficients can be determined from the boundary conditions (11) and (12) on the spheroidal interface ($\xi = \xi_0$). By substitute equations (13) and (14) into equations (11) and (12), the coupled unknown coefficients can be solved uniquely.

The spheroidal angular function $S_{mn}(c, \eta)$ depends not only on the angular variable η but also on the characteristics of the medium $c = kd$, where k is the propagation constant and d is the semi-focal length of the spheroid. Therefore, the equations used to determine the unknown coefficients constitute an infinite system of coupled linear equations. The procedure of obtaining such a system of linear equations for the unknown coefficients starts by applying the boundary conditions. Then the dyadic Green's functions equations (13) and (14) are substituted into the boundary conditions (11) and (12), respectively. The resulting equations based on (11)–(14) must hold for all allowed values of $0 \le \phi \le 2\pi$ and $-1 \le \eta \le 1$. We can make use of the orthogonality of the trigonometric functions by multiplying throughout by $\sin(m+1)\phi$ or $\cos(m+1)\phi$ where $m \ge 0$, and then by integrating them with respect to ϕ from 0 to 2π. Next, to remove the η-dependence of the equations, we make use of the orthogonal properties of the spheroidal angular functions. This is done by multiplying both sides of η-components by

$$\left(\xi_0^2 - \eta^2\right)^{\frac{2}{5}} \sqrt{\left(1-\eta^2\right) / \left(\xi_0^2 - 1\right)} = \left[\left(\xi_0^2 - 1\right) + \left(1 - \eta^2\right)\right]^{\frac{2}{5}} \sqrt{\left(1-\eta^2\right) / \left(\xi_0^2 - 1\right)}. \quad (15)$$

The equations that stand for the continuity of ϕ-components are multiplied by

$$\left(\xi_0^2 - \eta^2\right) \sqrt{\left(1-\eta^2\right)} = \left[\left(\xi_0^2 - 1\right) + \left(1 - \eta^2\right)\right] \sqrt{\left(1-\eta^2\right)}. \quad (16)$$

These multipliers are positive in the full range of η. Replace all the factors that are functions of η by series of the associated Legendre functions of the first kind, which are orthogonal functions in the interval $-1 \le \eta \le 1$ [22, 23]. After integrating both sides over the complete range of $\eta \in [-1, 1]$, an infinite system of equations satisfied by an infinite set of unknown scattering coefficients is obtained.

With these parameters, the equations for determining the unknown coefficients of the dyadic Green's functions in the prolate spheroidal system are now written for each value of m, in the following

forms:

$$\sum_{n=m}^{\infty} K_{\substack{e\\o}mn} \times \begin{pmatrix} \mp u^{+(3),t}_{\substack{e\\o}mn\eta}(c_1) & \nu^{+(3),t}_{\substack{o\\e}mn\eta}(c_1) & \pm u^{+(1),t}_{\substack{e\\o}mn\eta}(c_2) & -\nu^{+(1),t}_{\substack{o\\e}mn\eta}(c_1) \\ u^{+(3),t}_{\substack{e\\o}mn\varphi}(c_1) & \mp\nu^{+(3),t}_{\substack{o\\e}mn\varphi}(c_1) & -u^{+(1),t}_{\substack{e\\o}mn\varphi}(c_2) & \pm\nu^{+(1),t}_{\substack{o\\e}mn\varphi}(c_1) \\ \nu^{+(3),t}_{\substack{e\\o}mn\eta}(c_1) & \pm u^{+(3),t}_{\substack{o\\e}mn\eta}(c_1) & -\rho\nu^{+(1),t}_{\substack{e\\o}mn\eta}(c_2) & \mp\rho u^{+(1),t}_{\substack{o\\e}mn\eta}(c_1) \\ \pm\nu^{+(3),t}_{\substack{e\\o}mn\varphi}(c_1) & u^{+(3),t}_{\substack{o\\e}mn\varphi}(c_1) & \mp\rho\nu^{+(1),t}_{\substack{e\\o}mn\varphi}(c_2) & -\rho u^{+(1),t}_{\substack{o\\e}mn\varphi}(c_1) \end{pmatrix} \begin{pmatrix} A^{+xM}_{\substack{e\\o}mn} \\ A^{+xN}_{\substack{o\\e}mn} \\ B^{+xM}_{\substack{e\\o}mn} \\ B^{+xN}_{\substack{o\\e}mn} \end{pmatrix} = \sum_{n=m}^{\infty} K_{\substack{e\\o}mn} \begin{pmatrix} \mp u^{+(3),t}_{\substack{e\\o}mn\eta}(c_2) \\ u^{+(3),t}_{\substack{e\\o}mn\varphi}(c_2) \\ \rho\nu^{+(3),t}_{\substack{e\\o}mn\eta}(c_2) \\ \pm\rho\nu^{+(3),t}_{\substack{e\\o}mn\varphi}(c_2) \end{pmatrix} \tag{17}$$

$$\sum_{n=m}^{\infty} K_{\substack{e\\o}mn} \times \begin{pmatrix} \pm u^{-(3),t}_{\substack{e\\o}mn\eta}(c_1) & \nu^{-(3),t}_{\substack{o\\e}mn\eta}(c_1) & \mp u^{-(1),t}_{\substack{e\\o}mn\eta}(c_2) & -\nu^{-(1),t}_{\substack{o\\e}mn\eta}(c_1) \\ u^{-(3),t}_{\substack{e\\o}mn\varphi}(c_1) & \pm\nu^{-(3),t}_{\substack{o\\e}mn\varphi}(c_1) & -u^{-(1),t}_{\substack{e\\o}mn\varphi}(c_2) & \mp\nu^{-(1),t}_{\substack{o\\e}mn\varphi}(c_1) \\ \nu^{-(3),t}_{\substack{e\\o}mn\eta}(c_1) & \mp u^{-(3),t}_{\substack{o\\e}mn\eta}(c_1) & -\rho\nu^{-(1),t}_{\substack{e\\o}mn\eta}(c_2) & \pm\rho u^{-(1),t}_{\substack{o\\e}mn\eta}(c_1) \\ \mp\nu^{-(3),t}_{\substack{e\\o}mn\varphi}(c_1) & u^{-(3),t}_{\substack{o\\e}mn\varphi}(c_1) & \pm\rho\nu^{-(1),t}_{\substack{e\\o}mn\varphi}(c_2) & -\rho u^{-(1),t}_{\substack{o\\e}mn\varphi}(c_1) \end{pmatrix} \begin{pmatrix} A^{-xM}_{\substack{e\\o}mn} \\ A^{-xN}_{\substack{o\\e}mn} \\ B^{-xM}_{\substack{e\\o}mn} \\ B^{-xN}_{\substack{o\\e}mn} \end{pmatrix} = \sum_{n=m}^{\infty} K_{\substack{e\\o}mn} \begin{pmatrix} \pm u^{-(3),t}_{\substack{e\\o}mn\eta}(c_2) \\ u^{-(3),t}_{\substack{e\\o}mn\varphi}(c_2) \\ \rho\nu^{-(3),t}_{\substack{e\\o}mn\eta}(c_2) \\ \mp\rho\nu^{-(3),t}_{\substack{e\\o}mn\varphi}(c_2) \end{pmatrix} \tag{18}$$

In equations (17) and (18), ρ denotes $\sqrt{\varepsilon_1/\varepsilon_2}$; $c_i (i = 1, 2)$ denotes $k_i d$, where k_i is the propagation constant of region i and d is the semi-focal distance of the spheroid; $K_{\substack{e\\o}mn}$ denotes $\int\int\int_v \frac{2-\delta_{m0}}{N_{mn}} \psi^{(1)}_{\substack{e\\o}mn}(c_2, \boldsymbol{r}') \boldsymbol{M}_s(\boldsymbol{r}') dv'$, where δ_{m0} is the Kronker delta,

$N_{mn} = 2\sum_{k=0,1}^{\infty}{}' \frac{(k+2m)!(d_k^{mn})^2}{(2k+2m+1)k!}$ is the normalization factor of the angular function of the first kind [22, 25], and $\psi_{\substack{e\\o}mn}(c_2, \boldsymbol{r}') = S_{mn}(c_2, \eta')R_{mn}^{(1)}(c, \xi')^{\cos}_{\sin}m\phi'$ is the scalar spheroidal eigenfunctions; the elements of the matrices are given as follows [22]:

$$u_{\substack{e\\o}mn\eta}^{\pm(i),t}(c) = \left[\frac{dR_{mn}^{(i)}(c,\,\xi_0)}{d\xi_0} \mp \frac{m\xi_0}{\xi_0^2-1}R_{mn}^{(i)}(c,\,\xi_0)\right] \times \left[\left(\xi_0^2-1\right)^2 I_{t,1}^{mn}(c) + 2\left(\xi_0^2-1\right)I_{t,2}^{mn}(c) + I_{t,3}^{mn}(c)\right] \quad (19)$$

$$u_{\substack{e\\o}mn\phi}^{\pm(i),t}(c) = \frac{dR_{mn}^{(i)}(c,\,\xi_0)}{d\xi_0}I_{t,5}^{mn}(c) + \xi_0 R_{mn}^{(1)}(c,\,\xi_0)I_{t,8}^{mn}(c) \quad (20)$$

$$\begin{aligned}\nu_{\substack{e\\o}mn\eta}^{\pm i,t}(c) = \frac{1}{c}\Bigg\{&\left[\left(\left(\xi_0^2-1\right)\left(\lambda_{mn} - c^2\xi^2 + \frac{m^2}{\xi_0^2-1}\right) - 2m\,(m\pm 1)\right)\right.\\ &\left.\cdot\, R_{mn}^{(i)}(c,\,\xi_0) - \xi_0\left(\xi_0^2-1\right)\frac{dR_{mn}^{(i)}(c,\,\xi_0)}{d\xi_0}\right]\cdot\; I_{t,5}^{mn}(c)\\ &\mp\left[(m\pm1)\left(\xi_0^2-1\right)\cdot R_{mn}^{(i)}(c,\,\xi_0)\right]I_{t,7}^{mn} + \left[\left(\lambda_{mn} - c^2\xi^2\right.\right.\\ &\left.\left.\mp\frac{m}{\xi_0^2-1}\right)R_{mn}^{(i)}(c,\,\xi_0) + \xi_0\frac{dR_{mn}^{(i)}(c,\,\xi_0)}{d\xi_0}\right]\cdot\; I_{t,6}^{mn}(c)\\ &+\left[\xi_0\left(\xi_0^2-1\right)\frac{dR_{mn}^{(i)}(c,\,\xi_0)}{d\xi_0} - (3\pm 2m)\,R_{mn}^{(i)}\,(c,\,\xi_0)\right]\\ &\cdot\; I_{t,8}^{mn}(c) + \left[\xi_0\frac{dR_{mn}^{(i)}(c,\,\xi_0)}{d\xi_0} + \left(2\mp\frac{m}{\xi_0^2-1}\right)\cdot R_{mn}^{(i)}(c,\,\xi_0)\right]\\ &\cdot\; I_{t,9}^{mn}(c) - \left[m(m\pm1)(\xi_0^2-1)R_{mn}^{(i)}(c,\,\xi_0)\right]\cdot I_{t,4}^{mn}(c)\Bigg\}\end{aligned} \quad (21)$$

$$\begin{aligned}\nu_{\substack{e\\o}mn\phi}^{\pm(i),t}(c) = \frac{1}{c}\Bigg\{&\left[m\,(m\pm1)\,R_{mn}^{(i)}(c,\,\xi_0)\right]I_{t,0}^{mn}(c)\\ &+\left[(1\pm m)\,R_{mn}^{(i)}(c,\,\xi_0)\right]I_{t,10}^{mn}(c) - \left[c^2R_{mn}^{(i)}(c,\,\xi_0)\right]\\ &\cdot\; I_{t,2}^{mn}(c) + \left[\left(-c^2\left(\xi_0^2-1\right) + \frac{m(m\pm1)}{\xi_0^2-1}\right)R_{mn}^{(i)}(c,\,\xi_0)\right]\end{aligned}$$

$$\cdot\ I_{t,2}^{mn}(c) - \left[(1 \pm m)\,\xi_0 \frac{dR_{mn}^{(i)}(c,\,\xi_0)}{d\xi_0}\right] \cdot\ I_{t,1}^{mn}(c)\Bigg\} \tag{22}$$

$$u_{\substack{e\\o}mn\eta}^{z(i),t}(c) = mR_{mn}^{(i)}(c,\,\xi_0) \cdot \left[\left(\xi_0^2-1\right)^2 I_{t,4}^{mn}(c) + 2\left(\xi_0^2-1\right)^2 I_{t,5}^{mn}(c) + I_{t,6}^{mn}(c)\right] \tag{23}$$

$$u_{\substack{e\\o}mn\phi}^{z(i),t}(c) = R_{mn}^{(i)}(c,\,\xi_0)\cdot I_{t,11}^{mn}(c) - \left[\xi_0 \frac{dR_{mn}^{(i)}(c,\,\xi_0)}{d\xi_0}\right]\cdot I_{t,2}^{mn}(c) \tag{24}$$

$$\begin{aligned}\nu_{\substack{e\\o}mn\eta}^{\pm x(i),t}(c) = \frac{1}{c}\Bigg\{ & \left[\left(\xi_0^2-1\right)^2 \frac{dR_{mn}^{(i)}(c,\,\xi_0)}{d\xi_0}\right]\cdot I_{t,10}^{mn}(c) \\ & + \left[\left(\xi_0^2-1\right)\frac{dR_{mn}^{(i)}(c,\,\xi_0)}{d\xi_0} + 2\xi_0 R_{mn}^{(i)}(c,\,\xi_0)\right]\cdot I_{t,11}^{mn}(c) \\ & - \left(\xi_0^2-1\right)\left[\xi_0\left(\lambda_{mn} - c^2\xi^2 - \frac{m^2}{\xi_0^2-1}\right)R_{mn}^{(i)}(c,\,\xi_0)\right. \\ & \left. - \left(\xi_0^2-1\right)\cdot\frac{dR_{mn}^{(i)}(c,\,\xi_0)}{d\xi_0}\right]\cdot I_{t,1}^{mn}(c) \\ & - \left[\xi_0\left(\lambda_{mn} - c^2\xi^2\right)R_{mn}^{(i)}(c,\,\xi_0) + \left(\xi_0^2-1\right)\times\frac{dR_{mn}^{(i)}(c,\,\xi_0)}{d\xi_0}\right] \\ & \cdot I_{t,2}^{mn}(c) + \left[m^2\xi_0\left(\xi_0^2-1\right)\cdot R_{mn}^{(i)}(c,\,\xi_0)\right]\cdot\ I_{t,0}^{mn}(c)\Bigg\}\end{aligned} \tag{25}$$

$$\nu_{\substack{e\\o}mn\phi}^{z(i),t}(c) = \frac{m}{c}\left\{\left[\frac{\xi_0}{\xi_0^2-1}R_{mn}^{(i)}(c,\,\xi_0)\right]\cdot I_{t,8}^{mn}(c) + \left[\frac{dR_{mn}^{(i)}(c,\,\xi_0)}{d\xi_0}\right]\cdot I_{t,5}^{mn}(c)\right\} \tag{26}$$

where the coefficients $I_{t,l}^{mn}(c)$ ($t = 0, 1, 2, \ldots, 11$ and $l = 0, 1, 2, \ldots, 11$) are provided in a closed form in [21–23].

The system of linear equations (17) and (18) are valid for each value of t, so that taking t sufficiently large an adequate number of relations between unknown coefficients is generated. The convergence of the infinite series is expected both physically and mathematically. Practically, the infinite system of equations is truncated to a finite number of equations. According to Sinha and MacPhie [24], this

truncated number is taken as N_t =Integer ($|kb| + 4$) (where k is the propagation constant in the media, b is the major semi-axial length of the spheroid). In other words, there exist $4 \times N_t$ scalar unknowns for each of the above matrix systems. Assuming that the index t in the equations is taken as 0, 1, ..., $N_t - 1$, we can obtain a $4N_t \times 4N_t$ matrix system, and determine accurately these $4 \times N_t$ unknowns.

Because of the non-existence of orthogonality of spheroidal wave functions, the unknown scattering coefficients are coupled to each other. By using the method of functional expansion, the coupled unknowns are then determined explicitly from the matrix system of the linear equations. It should be noted that the source information is also included in the coupled equations. And the unknowns cannot be obtained analytically from the equations without evaluating the integrals of the slot current. This is different from the spherical case, where the transmitting and scattering coefficients are integrals of source currents and decoupled from each other.

The configuration of the prolate hemispheroidal DRA, shown in Fig. 1, is excited by a narrow slot. The narrow rectangular slot is parallel to the x-axis at the centre of the dielectric spheroid. At the opening, the field is approximated by the dominant TE_{111} mode. The electric field $\boldsymbol{E}_s$ in the slot along the x-axis is assumed to be y-directed, and vanishes at the ends of the slot. Also, the electric field is assumed not to vary across the narrow width of the slot. Thus

$$\boldsymbol{E}_s = \hat{y} E_0 \cos\left(\frac{\pi}{l} x'\right) \qquad \begin{cases} -l/2 \le x' \le l/2 \\ -w/2 \le y' \le w/2 \end{cases} \tag{27}$$

As discussed in Section 2, image theory is used to remove the ground plane to obtain an equivalent problem of a full dielectric prolate spheroid, excited by $\boldsymbol{M}_s = 2\boldsymbol{M}$, as shown in Fig. 2. The equivalent magnetic current is x-directed and only varies in x-direction. It is

$$\boldsymbol{M}_s = \begin{cases} -2\hat{z} \times \boldsymbol{E}_s = \hat{x} 2E_0 \cos\left(\dfrac{\pi}{l} x'\right) & \begin{cases} -l/2 \le x' \le l/2 \\ -w/2 \le y' \le w/2 \end{cases} \\ 0 & \textit{elsewhere} \end{cases} \tag{28}$$

Since the source current distribution has only the x-component, only the x-component of the dyadic Green's functions is needed.

2.3. Far Field Expression

For electromagnetic far field, we can simplify the expression (3) of the radiated field using the asymptotic form of spheroidal radial function

when $c\xi \to \infty$ [25]. After some tedious manipulation, the electric far field can be expressed as

$$\begin{aligned} E_\eta = \frac{-ik_2}{\pi d c_1^2 \xi} \sum_{n=0}^{\infty} \sum_{m=0}^{n} \Bigg\{ & \left(c_1^2 S_{mn} + c_1 S_{mn} + 1 \right) \cdot e^{i[c_1\xi - \frac{1}{2}(n+1)\pi]} \\ & \cdot \Big[A_e^{+xM} \cdot \sin\left((m+1)\,\phi\right) - A_e^{-xM} \cdot \sin\left((m-1)\,\phi\right) \\ & - A_o^{+xN} \cdot \sin\left((m+1)\,\phi\right) \cdot (\rho_1 + \rho_2) + A_o^{-xN} \\ & \cdot \sin\left((m+1)\,\phi\right) \cdot (\rho_1 + \rho_2) \Big] \cdot \iiint_v \Gamma_{mn} M_x\left(\boldsymbol{r}'\right) dv' \Bigg\} \end{aligned} \tag{29}$$

$$\begin{aligned} E_\phi = \frac{-ik_2}{\pi d c_1^2 \xi} \sum_{n=0}^{\infty} \sum_{m=0}^{n} \Bigg\{ & \left(-c_1^2 \eta S_{mn} + c_1 \eta S_{mn} + 1 \right) \cdot e^{i[c_1\xi - \frac{1}{2}(n+1)\pi]} \\ & \cdot \Big[A_e^{+xM} \cdot \cos\left((m+1)\,\phi\right) - A_e^{-xM} \cdot \cos\left((m-1)\,\phi\right) \\ & - A_o^{+xN} \cdot \cos\left((m+1)\,\phi\right) \cdot (\rho_3 + \rho_4) + A_o^{-xN} \\ & \cdot \cos\left((m+1)\,\phi\right) \cdot (\rho_3 + \rho_4) \Big] \cdot \iiint_v \Gamma_{mn} M_x\left(\boldsymbol{r}'\right) dv' \Bigg\} \end{aligned} \tag{30}$$

where the prime symbol denotes the source point location; M_x is the magnetic current distribution (28); A_e^{+xM}, A_e^{-xM}, A_e^{+xN}, and A_e^{-xN} are scattering coefficients, which can be determined by equations (17) and (18); Γ_{mn}, ρ_1, ρ_2, ρ_3, ρ_4, ρ_5, and ρ_6 are given by

$$\Gamma_{mn} = \frac{2 - \delta_{m0}}{N_{mn}} \psi^{(1)}_{\substack{e \\ o} mn}(c_2 \boldsymbol{r}') \tag{31}$$

$$\rho_1 = \frac{m}{\xi^2} \cdot \frac{dS_{mn}}{d\eta} + \frac{m\eta}{\xi^2(1-\eta^2)} S_{mn} \tag{32}$$

$$\rho_2 = (c_1 + 1)\left(1 - \eta^2\right) \frac{dS_{mn}}{d\eta} + \left[c_1^2 \eta^2 + \frac{m^2 \eta}{\xi^2(1-\eta^2)} \right] S_{mn} \tag{33}$$

$$\rho_3 = \frac{\eta}{\xi^2} \cdot \frac{dS_{mn}}{d\eta} + \left[c_1^2 + \frac{m^2}{\xi^2(1-\eta^2)} \right] S_{mn} \tag{34}$$

$$\rho_4 = \frac{m\eta}{\xi^2} \cdot \frac{dS_{mn}}{d\eta} + \frac{m\eta^2}{\xi^2(1-\eta^2)} S_{mn} \tag{35}$$

$$\begin{aligned} \rho_5 = & -(c_1 + 1)\eta(1-\eta^2)^{\frac{1}{2}} \frac{dS_{mn}}{d\eta} \\ & + \frac{m^2(\xi - 1) - (c_1 + 1)(1 + \eta^2)\xi}{\xi^2(1-\eta^2)^{\frac{1}{2}}} S_{mn} \end{aligned} \tag{36}$$

$$\rho_6 = \frac{m + m\xi(c_1 + 1)}{\xi(1 - \eta^2)^{\frac{1}{2}}} S_{mn}. \tag{37}$$

3. RESULTS AND DISCUSSION

In this section, radiation patterns of the hemispheroidal DRA excited by slot aperture with different parameters are presented. To check the validity of the formulation and associated software, numerical results when the axial ratio approaches one are compared with published data [9] of the corresponding hemispherical DRA. Also, the validity of the solution is examined by comparing the numerical results with Ansoft HFSS [19] simulation results.

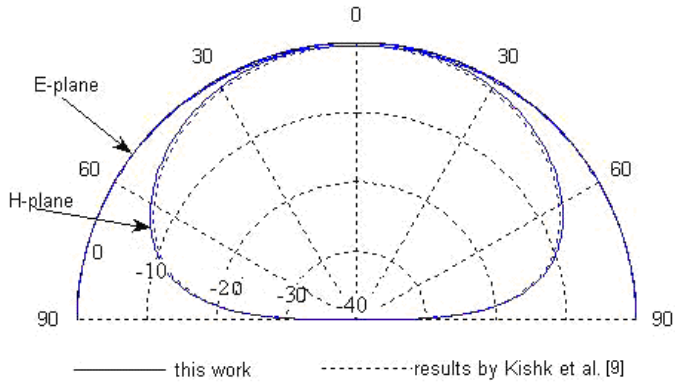

Figure 3. Radiation patterns (in dB) of DRAs with $a = 2.975\,\text{cm}$, $L = 5.0\,\text{cm}$, $W = 0.06\,\text{cm}$, $= 6.49$, and $f = 1.375\,\text{GHz}$. Solid line denotes patterns of hemispheroidal DRA (b/a=1.001) of this work, and dash line denotes patterns of a hemispherical DRA [9].

The relative radiation patterns calculated for the special case of $b/a \approx 1$ are shown in Fig. 3. Also shown are the corresponding hemispherical DRA results calculated by Kishk *et al.* [9]. It can be noted that our results are in a good agreement with Kishk's results. Another test case for the validity and accuracy of the solution is shown in Fig. 4 for a spheroidal DRA with $b/a = 1.15$. The calculated radiation patterns are in very good agreement with Ansoft HFSS simulation results.

To examine the effects of the axial ratio b/a on the radiation field, H-plane and E-plane patterns for the prolate hemispheroidal DRA with different values of b/a are shown in Fig. 5. All the calculated patterns are normalized using same normalized factor. It can be noted

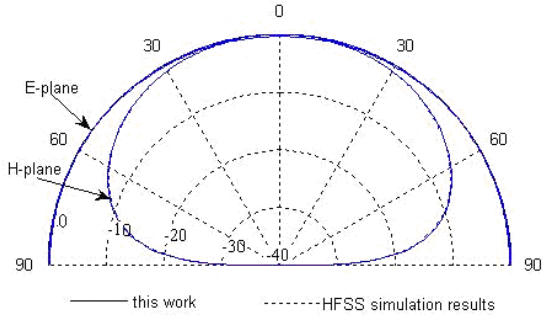

Figure 4. Radiation patterns (in dB) of a hemispheroidal DRA excited by a slot aperture, with $a = 2.975\,\text{cm}$, $b/a = 1.15$, $L = 5.0\,\text{cm}$, $W = 0.06\,\text{cm}$, $\varepsilon_r = 6.49$, and $f = 1.375\,\text{GHz}$. Solid line denotes results of hemispheroidal DRA of this work, and dash line denotes HFSS simulation results.

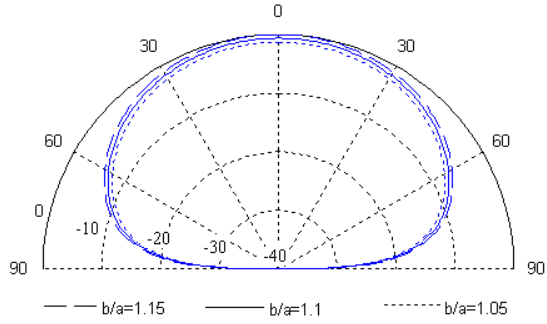

(a) H-plane patterns.

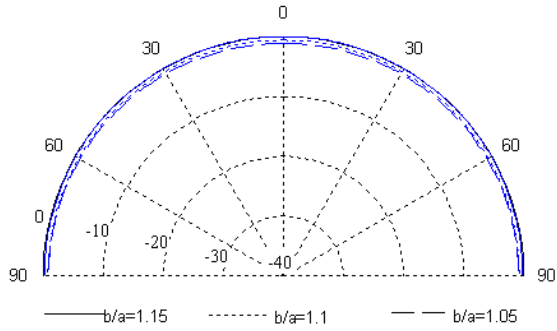

(b) E-plane patterns.

Figure 5. Calculated radiation patterns (in dB) of a hemispheroidal DRA excited by a slot aperture, with $a = 2.975\,\text{cm}$, $L = 5.0\,\text{cm}$, $W = 0.06\,\text{cm}$, $\varepsilon_r = 6.49$ and $f = 1.375\,\text{GHz}$ for different values of b/a.

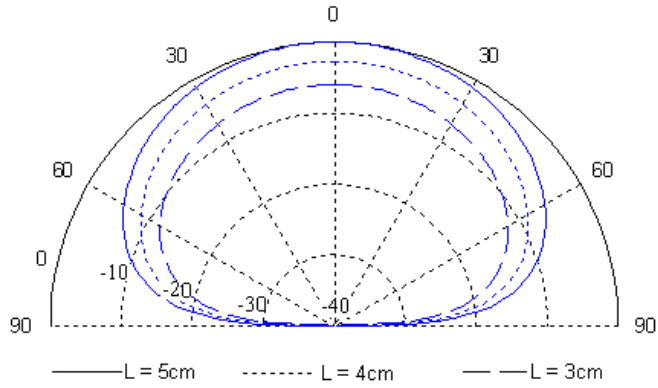

(a) H-plane patterns.

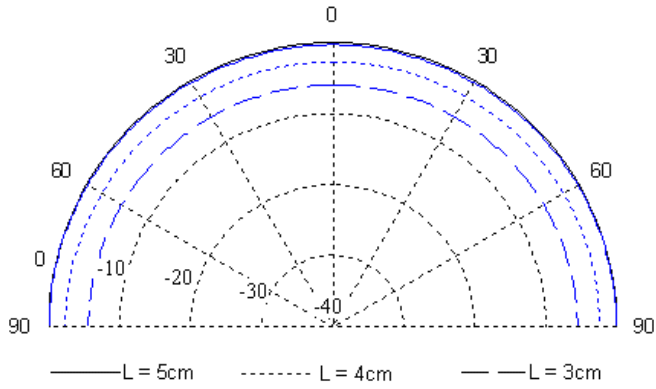

(b) E-plane patterns.

Figure 6. Calculated radiation patterns (in dB) of a hemispheroidal DRA excited by a slot aperture, with $a = 2.975\,\text{cm}$, $b/a = 1.15$, $W = 0.06\,\text{cm}$, $\varepsilon = 6.49$ and $f = 1.375\,\text{GHz}$ for different values of L.

that the beam width becomes wider when the ratio of b/a becomes larger. Therefore, when the slot length L is fixed, increasing the ratio of b/a increases the radiated power.

To examine the effects of the slot length (L) on the radiation field, H-plane and E-plane patterns for the prolate hemispheroidal DRA with different values of L are illustrated in Fig. 6. Again, all the calculated patterns are normalized using same normalized factor. These figures show that when the axial ration b/a is fixed, decreasing the slot length L decreases the radiated power.

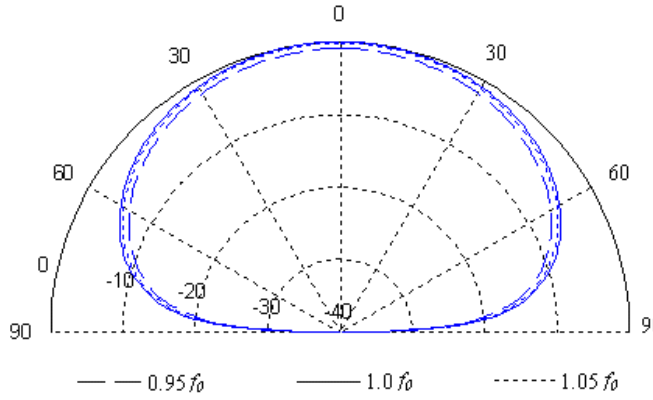

(a) H-plane patterns.

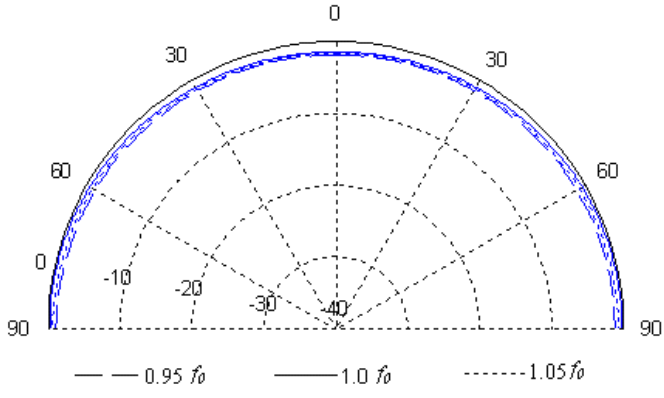

(b) E-plane patterns.

Figure 7. Calculated radiation patterns (in dB) of a hemispheroidal DRA excited by a slot aperture, with $a = 2.975\,\text{cm}$, $b/a = 1.5$, $W = 0.06\,\text{cm}$, $= 6.49$, $L = 5\,\text{cm}$ for different frequencies (f_0 is the resonant frequency).

Radiation patterns of the hemispheroidal DRA are calculated at resonant frequency (f_0) and other frequencies ($0.95\,f_0$ and $1.05\,f_0$). H-plane and E-plane patterns are shown in Fig. 7. It can be seen that the antenna radiates the most power at the resonant frequency with a variation of about 1 dB over the selected two frequency values.

4. CONCLUSION

In this work, the problem of radiation from a prolate hemispheroidal dielectric resonator antenna above an infinite ground and excited by a slot has been investigated using dyadic Green's function technique. The dyadic Green's functions are expressed in terms of the vector spheroidal wave functions with unknown scattering expansion coefficients. The unknown scattering coefficients of the dyadic Green's functions are obtained by enforcing the boundary conditions. Simple and compact far field expressions for the electric field are derived for a prolate hemispheroidal DRA excited by a slot with TE_{111} magnetic current distribution.

The validity of the solution was examined by comparing with HFSS simulation results and for the special case where the hemispheroid approaches the hemispherical shape ($b/a \approx 1$). Selected radiation pattern results were obtained for different parameters. The effect of the slot length and the shape of the spheroid on the radiation pattern were considered.

REFERENCES

1. Long, S. A., M. W. McAllister, and L. C. Shen, "The resonant cylindrical dielectric cavity antenna," *IEEE Trans. on Antenna Propagat.*, Vol. 31, 406–412, 1983.
2. McAllister, M. W., S. A. Long, and G. L. Conway, "Rectangular dielectric-resonator antenna," *Electronics Letters*, Vol. 19, 218–219, 1983.
3. McAllister, M. W. and S. A. Long, "Resonant hemispherical dielectric antenna," *Electronics Letters*, Vol. 20, 657–659, 1984.
4. Kishk, A. A., M. R. Zunoubi, and D. Kajfez, "A numerical study of a dielectric disc antenna above grounded dielectric substrate," *IEEE Trans. on Antenna Propagat.*, Vol. 41, No. 6, 813–821, 1993.
5. Kishk, A. A., A. Ittipiboon, Y. M. M. Antar, and M. Cuhaci, "Dielectric resonator antennas fed by a slot in the ground plane of a microstrip line," *Eighth International Conference on Antennas and Propagation*, Vol. 1, 540–543, 1993.
6. Leung, K. W., K. M. Luk, K. Y. A. Lai, and D. Lin, "Theory and experiment of a coaxial probe fed hemispherical dielectric resonator antenna," *IEEE Trans. on Antenna Propagat.*, Vol. 41, 1390–1398, Oct. 1993.
7. Leung, K. W., K. K. Tse, K. M. Luk, and E. K. N. Yung, "Cross-polarization characteristics of a probe-fed hemispherical dielectric

resonator antenna," *IEEE Trans. on Antenna Propagat.*, Vol. 47, 1228–1230, July 1999.

8. Leung, K. W., K. Y. A. Lai, K. M. Luk, and D. Lin, "Input impedance of aperture coupled hemispherical dielectric resonator antenna," *Electronics Letters*, Vol. 29, 1165–1167, June 1993.
9. Kishk, A. A., G. Zhou, and A. W. Glisson, "Analysis of dielectric-resonator antennas with emphasis on hemispherical structures," *IEEE Antennas and Propagation Magazine*, Vol. 36, 20–31, April 1994.
10. Leung, K. W., K. M. Luk, K. Y. Chow, and E. K. N. Yung, "Bandwidth enhancement of dielectric resonator antenna by loading a low-profile dielectric disk of very high permittivity," *Electronics Letters*, Vol. 33, 725–726, April 1997.
11. Lee, M. T., K. M. Luk, E. K. N. Yung, and K. W. Leung, "Circularly polarised dielectric resonator antenna with a microstrip feed," *Microwave Conference, Asia Pacific 1999*, Vol. 3, 722–723, 1999.
12. Leung, K. W., W. C. Wong, K. M. Luk, and E. K. N. Yung, "Circular-polarised dielectric resonator antenna excited by dual conformal strips," *Electronics Letters*, Vol. 36, 484–486, 2000.
13. Wong, W. C., K. W. Leung, K. M. Luk, and E. K. N. Yung, "Circular-polarized dielectric resonator antenna excited by dual conformal strips," *IEEE Antennas and Propagation Society International Symposium*, Vol. 2, 1021–1025, July 2000.
14. Mongia, R. K., A. Ittipiboon, Y. M. M. Antar, P. Bhartia, and M. Cuhaci, "A half-split cylindrical dielectric resonator antenna using slot-coupling," *IEEE Microwave and Guided Wave Letters*, Vol. 3, No. 2, Feb. 1993.
15. Salameh, M., Y. M. M. Antar, and G. Seguin, "Coplanar-waveguide-fed slot-coupled rectangular dielectric resonator antenna," *IEEE Trans. on Antenna Propagat.*, Vol. 50, 1415–1419, Oct. 2002.
16. Oliver, M. B., Y. M. M. Antar, R. K. Mongia, and A. Ittipiboon, "Circularly polarised rectangular dielectric resonator antenna," *Electronics Letters*, Vol. 31, 418–419, March 1995.
17. Kishk, A. A., "Wide-band truncated tetrahedron dielectric resonator antenna excited by a coaxial probe," *IEEE Trans. on Antenna Propagat.*, Vol. 51, 2913–2917, Oct. 2003.
18. Lo, H. Y., K. W. Leung, K. M. Luk, and E. K. N. Yung, "Low profile equilateral-triangular dielectric resonator antenna of very high permittivity," *Electronics Letters*, Vol. 35, No. 25, 2164–2166,

Dec. 1999.

19. *Ansoft High Frequency Structures Simulator (HFSS)*, Version 9.0, Ansoft Corporate.
20. Tai, C. T., *Dyadic Green's Functions in Electromagnetic Theory*, 2nd Ed., IEEE Press, Piscataway, NJ, 1994.
21. Li, L.-W., X. K. Kang, and M. S. Leong, *Spheroidal Wave Functions in Electromagnetic Theory*, John Wiley & Sons, Inc., 2002.
22. Li, L.-W., M. S. Leong, P.-S. Kooi, and T.-S. Yeo, "Spheroidal vector wave eigenfunction expansion of dyadic Green's functions for a dielectric spheroid," *IEEE Trans. On Antenna Propagat.*, Vol. 49, 645–659, April 2001.
23. Asano, S. and G. Yamamoto, "Light scattering by a spheroidal particle," *Appl. Opt.*, Vol. 14, 29–49, 1975.
24. Sinha, B. P. and R. H. MacPhie, "Electromagnetic scattering by prolate spheroids for plane waves with arbitrary polarization and angle of incidence," *Radio Sci.*, Vol. 12, 171–184, 1977.
25. Flammer, C., *Spheroidal Wave Functions*, Stanford University Press, Stanford, CA, 1957.